AD-A052 836 COLORADO STATE UNIV FORT COLLINS DEPT OF CHEMISTRY F/G 7/4
ANALYTICAL IMPLICATIONS OF DIFFERENTIAL PULSE POLAROGRAPHY OF I--ETC(U)
APR 78 J W DILLARD, J J O'DEA, R A OSTERYOUNG N00014-77-C-0004
UNCLASSIFIED TR-6 NL

| OF |
ADA
052836

END
DATE
FILMED
5-78
DDC

OFFICE OF NAVAL RESEARCH

Contract N00014-77-C-0004

TECHNICAL REPORT NO. 6

ANALYTICAL IMPLICATIONS OF DIFFERENTIAL PULSE POLAROGRAPHY OF IRREVERSIBLE REACTIONS FROM DIGITAL SIMULATION; CALCULATIONS AND EXPERIMENTS

by

James W. Dillard*, John J. O'Dea and R. A. Osteryoung

Prepared for Publication in

Analytical Chemistry

Department of Chemistry
Colorado State University
Fort Collins, Colorado 80523

April, 1978

*Present Address: Tennessee Valley Authority, River Oaks Building, Muscle Shoals, Alabama 35660

Unclassified

SECURITY CLASSIFICATION OF THIS PAGE (When Data Entered)

REPORT DOCUMENTATION PAGE

READ INSTRUCTIONS BEFORE COMPLETING FORM

1. REPORT NUMBER: Technical Report, No. 6
2. GOVT ACCESSION NO.: TR-6
3. RECIPIENT'S CATALOG NUMBER:

4. TITLE (and Subtitle): Analytical Implications of Differential Pulse Polarography of Irreversible Reactions from Digital Simulation; Calculations and Experiments.

5. TYPE OF REPORT & PERIOD COVERED: Interim

6. PERFORMING ORG. REPORT NUMBER:

7. AUTHOR(s): James W. Dillard, John J. O'Dea and R. A. Osteryoung

8. CONTRACT OR GRANT NUMBER(s): N00014-77-C-0004

9. PERFORMING ORGANIZATION NAME AND ADDRESS:
Department of Chemistry
Colorado State University
Fort Collins, CO 80523

10. PROGRAM ELEMENT, PROJECT, TASK AREA & WORK UNIT NUMBERS:

11. CONTROLLING OFFICE NAME AND ADDRESS:
Chemistry Program
Office of Naval Research
Arlington, VA 22217

12. REPORT DATE: April 1978

13. NUMBER OF PAGES: 30

14. MONITORING AGENCY NAME & ADDRESS (if different from Controlling Office):
Office of Naval Research
Resident Representative
Suite 210, 6740 E. Hampden Avenue
Denver, CO 80222

15. SECURITY CLASS. (of this report): Unclassified

15a. DECLASSIFICATION/DOWNGRADING SCHEDULE:

16. DISTRIBUTION STATEMENT (of this Report)

Approved for Public Release; Distribution Unlimited

17. DISTRIBUTION STATEMENT (of the abstract entered in Block 20, if different from Report)

18. SUPPLEMENTARY NOTES

Prepared for publication in Analytical Chemistry

19. KEY WORDS (Continue on reverse side if necessary and identify by block number)

differential pulse polarography; irreversible reactions; digital simulations;

20. ABSTRACT (Continue on reverse side if necessary and identify by block number)

Explicit finite difference simulations of differential pulse polarography have been developed for evaluating the analytical applications of differential pulse polarography to irreversible and quasireversible electron transfer reactions. From simulation data, detailed prediction of polarographic peak shape and position as a function of pulse height, pulse time and drop time is possible. Optimum conditions for analytical application of differential pulse polarography are discussed.

DD FORM 1 JAN 73 1473 EDITION OF 1 NOV 65 IS OBSOLETE

Unclassified

SECURITY CLASSIFICATION OF THIS PAGE (When Data Entered)

404 992

LB

Brief

Explicit finite difference simulations of differential pulse polarography for irreversible and quasireversible electron transfer reactions are used to evaluate signal response to parameter changes such as pulse height, pulse time and drop time. Experimental verification of predicted peak shoulders and dual peaks under certain electron transfer conditions is also included.

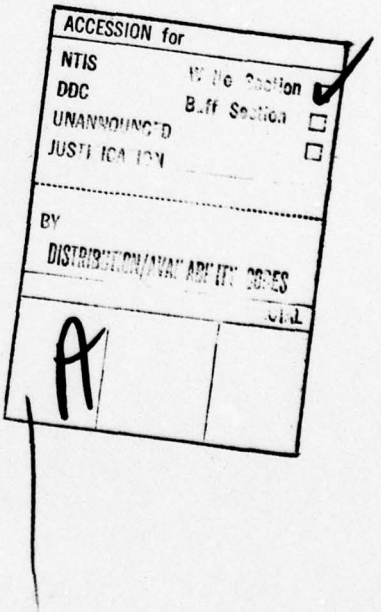

Abstract

Explicit finite difference simulations of differential pulse polarography have been developed for evaluating the analytical applications of differential pulse polarography to irreversible and quasireversible electron transfer reactions. From simulation data, detailed prediction of polarographic peak shape and position as a function of pulse height, pulse time and drop time is possible. Optimum conditions for analytical application of differential pulse polarography are discussed.

Differential pulse polarography has become an increasingly important tool in the analysis of both organic and inorganic electroactive species. With the expanded interest in differential pulse polarography, the systematic evaluation of the analytically important experimental parameters has become necessary. Such an evaluation for reversible electron transfer reactions has already been reported.[1] The treatment of irreversible and quasireversible systems will be presented here.

Previous coupling of an explicit finite difference simulation for differential pulse polarography with a standard nonlinear least squares fitting program has demonstrated the feasibility of studying electron transfer kinetics by differential pulse polarography.[2] However, the cost of executing such coupled programs usually limits the exhaustive investigation of complex electron transfer reactions. The ready availability of a mini-computer system in our laboratory normally used for on-line data acquisition prompted a feasibility study of using finite difference simulations to evaluate the analytical applications of differential pulse polarography. The execution time of these simulations was greatly reduced by the implementation of an incremental time change during the course of the simulation. The details of this expedited simulation technique have been previously published.[3]

The treatment of quasireversible systems dictates that electron transfer kinetics be included in the simulation model. This elaboration has been incorporated into our programs and will be discussed further in the theoretical section.

The use of this simulator enables the detailed prediction of polarographic peak shape and position as a function of controlled experimental variables such as pulse height, pulse time, and drop time. Such simulations promise to be of considerable aid to the analyst who wishes to select and optimize the experimental conditions of a differential pulse polarographic analysis without resort to lengthy empirical studies.

THEORETICAL

Digital simulation as a general method for solving electrochemical diffusion-kinetic problems has been discussed in detail by Feldberg.[4] A recent publication by Ruzic and Feldberg[5] described an improved simulation of the dropping mercury electrode (DME) with associated compression and sphericity. The simulator used in this investigation incorporates the improved DME model and the time change method mentioned earlier.

For electron transfer reductions of the type

$$OX + ne^- \underset{k_b}{\overset{k_f}{\rightleftharpoons}} RED \qquad (1)$$

the flux of the electron transfer reaction is calculated from Feldberg[4] (Equation 116)

$$ZZ = \frac{RATEHF*UU(1,1)-RATEHB*UU(2,1)}{1 + (RATEHF/2*DD)+(RATEHB/2*DD)} \qquad (2)$$

which is derived from the basic surface boundary conditions. The surface concentrations (UU(1,1), UU(2,1)) of OX and RED are in simulator units and are assumed to be soluble in the solution. The normalized diffusion coefficient (DD) has been optimized to a value of 0.4

simulator units. The potential dependent heterogeneous electron transfer rates (RATEHF and RATEHB) must be determined from the apparent standard heterogeneous rate constant. From the general form of the Butler-Volmer equation k_f and k_b may be deduced

$$k_f = k_a^\circ \exp\left(\frac{-\vec{\alpha}F}{RT}(E-E^\circ)\right) \tag{3}$$

$$k_b = k_a^\circ \exp\left(\frac{\overleftarrow{\alpha}F}{RT}(E-E^\circ)\right) \tag{4}$$

where

$$\vec{\alpha} = \vec{\gamma} + r\beta \tag{5}$$

$$\vec{\alpha} = n - \vec{\gamma} - r\beta \tag{6}$$

The symmetry factor β, the total number of electrons transferred n, and the number of charge transfer steps prior to the rate determining step $\vec{\gamma}$, must be supplied. For charge transfer reactions r = 1, and R, T and F have their usual significance. All simulations are referenced to $E^\circ = 0.0$ for convenience. The apparent heterogeneous rate constant k_a° and potential E must be converted into simulator units before they may be used in equation (3) or (4). The dimensionless relationship yielding the heterogeneous rate constant is described by the following

$$k_a^\circ * \sqrt{t/D} = \text{RATEHS} * \sqrt{\text{TMAX}/\text{DD}} \tag{7}$$

where t is the experimental time (ie. drop time) and D is the measured diffusion coefficient. TMAX and DD are the related simulator variables. Solving for RATEHS and substitution in equations (3) and (4) permits the calculation of RATEHF and RATEHB as a function of normalized potential. Using this method, simulations of multiple electron transfer reactions including the rate determining step are possible.

Different types of polarographic experiments are simulated by jumping the normalized potential at the appropriate times corresponding to the excitation waveform and sampling the simulated response to this perturbation. In order to theoretically evaluate the current-potential relationship for differential pulse polarography, the concentration profile prior to pulse application must be known. This is accomplished by using an explicit finite difference simulation to generate the concentration profile for dc polarography. This dc profile corresponds exactly to the differential pulse profile prior to pulse application. Hence, the simulated behavior prior to pulse application should lead to the standard known current profile behavior for irreversible processes. This prepulse dc behavior can be regarded as a verification of the simulator.

TAST POLAROGRAPHY

The current-voltage curves generated by the simulator for TAST polarography were analyzed by three methods and were found to be in close agreement with accepted theory. An apparent heterogeneous rate of 10^{-4} cm/sec and a symmetry factor of 0.5 were used to simulate TAST polarograms for n = 1, 2, 3 and all possible combinations for the rate determining step.

For irreversible electron transfer reactions, the current-potential curve at the foot of the wave may be expressed by

$$i \propto \exp(-\alpha n_a FE/RT) \qquad (8)$$

From the slope of the E versus log i plot for currents at the foot of the wave, a value for αn_a may be calculated. The resulting "Tafel" slope and αn_a values for the simulated TAST polarograms are listed in Table I.

From TAST polarograms, the ratio i/i_d may be used in determining the heterogeneous rate and transfer coefficient.[6] The value of λ

$$\lambda = k_f t^{1/2}/D_o^{1/2} \tag{9}$$

may be determined from tables calculated by Koutecky[7] in which

$$i/id = \pi^{1/2}\lambda \exp\lambda^2 \operatorname{erfc}\lambda \tag{10}$$

For several ratios of i/i_d, the values of k_f may be calculated. From a plot of log k_f versus potential, the transfer coefficient and heterogeneous rate may be determined

$$k_f = k_a^{\circ} \exp(-\alpha n_a FE/RT) \tag{11}$$

Table II compares the determined k_a° and αn_a values for the simulated TAST polarograms with the input values.

The simulated TAST polarograms were finally evaluated with a modified plot of log $i/(i_d - i)$ versus potential.[8] The following expression derived explicitly by Meites from Koutecky's $F(\lambda)$

$$E + 0.2412 = \frac{0.05915}{\alpha n_a} \log \frac{1.349 k_a^{\circ} + 1/2}{D_o^{1/2}} - \frac{0.0542}{\alpha n_a} \log \frac{i}{i_d - i} \tag{12}$$

may be separated into

$$E = E_{1/2} - \frac{0.0542}{\alpha n_a} \log \frac{i}{i_d - i} \tag{13}$$

and

$$E_{1/2} = -0.2412 + \frac{0.05915}{\alpha n_a} \log \frac{1.349 k_a^{\circ} + 1/2}{D_o^{1/2}} \tag{14}$$

A plot of log $i/(i_d - i)$ versus potential yields the value for αn_a which is used in equation (14) to calculate the heterogeneous rate. The determined αn_a and k_a° values are listed in Table III.

DIFFERENTIAL PULSE POLAROGRAPHY

The effect of changing heterogeneous rate constant upon peak current, peak potential and peak width for one electron reduction was studied. Figure 1 illustrates the relationship between peak current and log $k_a^\circ \sqrt{t}$ where t is the pulse time. For shorter pulse times, the break between quasireversible and reversible occurs at larger rates as would be expected. The spread observed in (A) for a large pulse height is reduced considerably in(B) for small pulse heights. At rates slower then 10^{-4} cm/sec essentially no change in peak height is observed as should be expected for irreversible electron transfer reactions. Figure 2 illustrates the same data as Figure 1 but plotted against log k_a°.

The pulse time dependence of current is depicted in Figure 3 for the reversible and irreversible cases. For large pulse times, the peak current approaches zero at the limit because the pulse current (current II) will be nearly equal to the dc current (current I) except for the difference in electrode area. At very short pulse times the peak current approaches infinity asymptotically. However, the experimental limit is a function of the charging current.

The dependence of peak current as a function of pulse height at short and long pulse times is illustrated in Figure 4. For small pulse heights, reversible electron transfer reactions define the upper current limit while the totally irreversible case defines the lower limit. These limits eventually converge and level off at the normal pulse limiting current for large pulse heights.

The observed peak potential behavior is depicted in Figure 5. For large heterogeneous rates the peak potential is shifted according to the magnitude of the pulse heights.

$$Epk = E_{1/2} - \frac{\Delta E}{2}$$

For rates slower than 10^{-3} cm/sec the change in peak potential is linear with a change of 120 mV per decade change in rate. This potential shift is analogous to the change in $E_{1/2}$ for TAST polarography[6] ($\alpha n_a = 0.5$)

$$E_{1/2} = \frac{RT}{\alpha n_a F} \log \frac{k_a^{\circ}}{\lambda^{1/2} D_o^{1/2}} + \frac{RT}{2\alpha n_a F} \log t$$

The observed peak separation for different pulse times shifts in the direction expected. For a given peak potential, a faster rate is represented at shorter pulse times than at longer pulse times.

The peak width at half height is plotted as a function of heterogeneous rate in Figure 6. For quasireversible electron transfers, a sharp change in width should be observed for small changes in rate. Once irreversibility is established little change in width occurs. Also for short drop times and long pulse times dc faradaic distortion broadens the observed peaks.

Simulations of multiple electron transfer reductions predicted unique differential pulse polarograms. A most interesting example is a two electron quasireversible reduction for symmetry factors in the 0.2 - 0.4 region. The four polarograms in Figure 7 illustrate the region of heterogeneous rate between 10^{-2} and 10^{-4} cm/sec for a two electron transfer with the first electron being the rate determining step (symmetry factor = 0.3). This behavior was not observed for large

symmetry factors or if the second electron was the rate determining step. Shoulders or second peaks have been noted under similar conditions for ac polarography[9].

EXPERIMENTAL

The minicomputer used for these simulations has been described previously.[3] An important feature of this system is the ability to display either the concentration profile or the current-time profile of the simulation during execution. This capability enables the user to perceive trends in the calculations immediately and hence allows for the rapid optimization of the simulation parameters. The finite difference simulator used in these studies is written in standard Fortran IV and is available upon request. The zinc diffusion coefficients (D_O and D_R) used in the simulation were assumed to equal the literature value of 7.2×10^{-6} cm^2/sec for infinity dilute solutions.[10]

The experimental zinc polarograms were obtained by using a custom built potentiostat employing fast settling Analog Devices 48J operational amplifiers. This potentiostat was interfaced to a Digital Equipment Corporation PDP-12 minicomputer which acquired the data by means of a 12-bit analogue to digital converter. The PDP-12 system also provided the excitation waveform to the potentiostat and controlled a PAR model 172A drop knocker which was attached to a conventional polarographic capillary. A commercially available saturated calomel electrode (Sargent Welch # 30080-15A) was used as the reference electrode. The counter electrode consisted of a platinum wire helix isolated from the bulk of the solution by a pyrex tube with a pinhole in the bottom. The

polarographic cell was constructed from quartz and Teflon and was thermoregulated at 25.0 ± 0.1°C. Triply distilled mercury (Bethlehem Apparatus Co.) was used in the dropping mercury electrode. All solutions were deaerated with prepurified nitrogen passed over a BASF catalyst bed to remove residual oxygen. The supporting electrolytes were prepared from stock solutions of reagent grade potassium nitrate. The zinc and cadmium concentrations were derived from EDTA standardized stock solutions. Deionized Millipore-Q water was used as the solvent.

RESULTS AND DISCUSSION

The kinetic parameters used in our simulations were obtained from the analysis of normal pulse and tast polarographic data according to Christie, et al.[11] The apparent heterogeneous rate constants were found to vary inversely with the supporting electrolyte concentration in agreement with previous studies.[12] The experimentally accessible range of rate constant for zinc reduction as a function of supporting electrolyte concentration for potassium nitrate is plotted in Figure 8. Unfortunately, the heterogeneous rate constants are not reduced enough even in saturated electrolytes to affect the clean separation of dual peaks as predicted by the simulations for sufficiently low rate constants. However, a pronounced tailing of the zinc peak is observed. Figure 9 shows typical experimental curves with superimposed simulations. Similar peak shapes have been previously published but without comment or explanation. Our simulations demonstrate that this tailing is due to the interplay of heterogeneous electron transfer kinetics and diffusion in this quasireversible system. A detailed comparison of

the experimental data with the theoretical predictions is presented in Table IV. The predicted peak width at half height and peak shifts are in good agreement with experiment. The shifts in zinc peak positions were measured against a cadmium spike in the supporting electrolyte in order to compensate for shifts due to changes in the reference junction potential from one electrolyte concentration to the next.

From the analytical point of view, the results of these experiments and simulations clearly show which parameters should be optimized for the best determinations of quasireversible and irreversible systems. In irreversible systems the sensitivity of differential pulse polarography is considerably reduced as compared to the reversible case. The resolution of adjacent peaks is also diminished due to large peak widths. Unfortunately, this method when applied to irreversible systems is relatively insensitive to parameter changes over the usual ranges available on commercial instrumentation. Little advantage is gained by changing the excitation potential waveform except that at large pulse heights and short pulse times, the largest peak currents are obtained. Under these conditions, however, the residual current due to the charging of the electrical double layer will constitute a significant fraction of the total current measured. Hence, a practical compromise between increased sensitivity and enhanced background must be reached by the analyst in selection of pulse height and pulse time.

In quasireversible systems, small changes in electrode kinetics can cause abrupt changes in peak shape and peak current. The reduction of zinc is an excellent example which illustrates this kinetic dependence. Large errors in the analytical determination of such systems may arise if the composition or concentration of the supporting electrolyte is

not carefully controlled. As with the irreversible systems, the use of large pulse heights and short pulse times will increase sensitivity. Longer drop times will also increase the peak current but at the expense of increased total analysis time. In addition, some improvement in resolution can be realized by using smaller pulse heights or by manipulation of the supporting electrolyte concentration. In the case of zinc, peak tailing is eliminated by decreasing the supporting electrolyte concentration. For the determination of quasireversible systems, a compromise between resolution, sensitivity, and total analysis time can be achieved by the prudent choice of experimental conditions. Simulations such as those presented here can aid the analyst in making those crucial choices.

CREDIT

This work was supported in part by the National Science Foundation under Grant CHE75-00332 and in part by the Office of Naval Research under Grant N00014-77-C-0004.

LITERATURE CITED

(1) E.P. Parry and R.A. Osteryoung, Anal. Chem., 37, 1634 (1965).

(2) James W. Dillard and K.W. Hanck, Anal. Chem., 48, 218 (1976).

(3) James W. Dillard, John A. Turner, and R.A. Osteryoung, Anal. Chem., 49, 1246 (1977).

(4) S.W. Feldberg, "Electroanalytical Chemistry", Vol. III, A. Bard, Ed., Marcel Dekker, New York, 1969, pp 199-296.

(5) I. Ruzic and S.W. Feldberg, J. Electroanal. Chem., 63, 1 (1975).

(6) P. Delahay, New Instrumental Methods in Electrochemistry, Interscience Pub., New York, 1954, Ch. 4.

(7) J. Koutecky, Chem. Listy, 47, 323 (1953).

(8) Louis Meites, Polarographic Techniques, Interscience Pub., New York, 1965, p 240.

(9) Donald E. Smith, "Electroanalytical Chemistry", Vol. I, A. Bard, Ed., Marcel Dekker, New York, 1969, pp 1, 155.

(10) R. Parsons, Handbook of Electrochemical Constants, Butterworths, London, 1959, p 79.

(11) J.H. Christie, E.P. Parry and R.A. Osteryoung, Electrochim. Acta 11, 1525 (1966).

(12) J. Koryta, Electrochim. Acta 6, 67 (1962).

TABLE I Kinetic Parameters for Simulated TAST Polarograms: E vs. log i

	Determined		Theoretical	
	Slope mV	αn_a	Slope mV	αn_a
n = 1	117.6	0.50	118.3	0.50
n = 2				
RDS = 1	120.3	0.49	118.3	0.50
RDS = 2	40.1	1.47	39.4	1.50
n = 3				
RDS = 1	120.3	0.49	118.3	0.50
RDS = 2	39.1	1.51	39.4	1.50
RDS = 3	24.3	2.40	23.7	2.50

RDS = rate determining step

TABLE II Kinetic Parameters for Simulated TAST Polarograms: Koutecky Method

	Determined		Theoretical	
	k_a°	αn_a	k_a°	αn_a
n = 1	0.197×10^{-4}	0.50	1.0×10^{-4}	0.50
n = 2				
RDS = 1	0.97×10^{-4}	0.50	1.0×10^{-4}	0.50
RDS = 2	0.95×10^{-4}	1.52	1.0×10^{-4}	1.50
n = 3				
RDS = 1	0.98×10^{-4}	0.50	1.0×10^{-4}	0.50
RDS = 2	0.97×10^{-4}	1.50	1.0×10^{-4}	1.50
RDS = 3	0.96×10^{-4}	2.52	1.0×10^{-4}	2.50

RDS = rate determining step

TABLE III Kinetic Parameters for Simulated TAST Polarograms: Meites Method

	Determined		Theoretical	
	k_a°	αn_a	k_a°	αn_a
n = 1	1.0×10^{-4}	0.50	1.0×10^{-4}	0.50
n = 2				
RDS = 1	0.99×10^{-4}	0.50	1.0×10^{-4}	0.50
RDS = 2	0.99×10^{-4}	1.50	1.0×10^{-4}	1.50
n = 3				
RDS = 1	1.0×10^{-4}	0.50	1.0×10^{-4}	0.50
RDS = 2	1.0×10^{-4}	1.50	1.0×10^{-4}	1.50
RDS = 3	0.98×10^{-4}	2.49	1.0×10^{-4}	2.50

RDS = rate determining step

TABLE IV Zinc Data

k_a°	Normalized Current		Peak Width Half-height, mV		E_{Zinc} vs $E_{Cadmium}$ mV	Theory E_{pk} vs E° mV
	Zn	Theory	Zn	Theory		
1.3×10^{-2}	1.0	1.0	59.8	54.5	-422	15.2
6.7×10^{-3}	0.71	0.72	63.5	58.5	-420	17.6
4.6×10^{-3}	0.50	0.56	69.2	61.4	-417	19.3
3.2×10^{-3}	0.40	0.42	68.7	64.9	-416	21.2

pulse time 16.67 msec
drop time 2 sec
pulse height 25 mV

FIGURES

(1) Peak current versus log $k_a^\circ \sqrt{t_{pulse}}$ for differential pulse polarography. Pulse height, (A) 100 mV, (B) 10 mV; Pulse time, (a) 10 msec, (b) 20 msec, (c) 40 msec, (d) 70 msec; Drop time 0.5 sec.

(2) Peak current versus log k_a° for differential pulse polarography. Pulse height, (A) 100 mV, (B) 10 mV; Pulse time, (a) 10 msec, (b) 20 msec, (c) 40 msec, (d) 70 msec; Drop time 0.5 sec.

(3) Peak current versus $\sqrt{t_{pulse}}$ for differential pulse polarography. Pulse height, (A) 100 mV, (B) 10 mV; Pulse time, (a) 10 msec, (b) 20 msec, (c) 40 msec, (d) 70 msec; Drop time 0.5 sec.

(4) Peak current versus E_{pulse} for differential pulse polarography. Pulse time, (A) 10 msec, (B) 70 msec; Apparent heterogeneous rate constant, (a) reversible, (b) 10^{-2} cm/sec, (c) 3×10^{-3} cm/sec, (d) 10^{-6} cm/sec; Drop time 0.5 sec.

(5) -log k_a° versus peak potential for differential pulse polarography. Pulse height, (a and b) 100 mV, (c and d) 10 mV; Pulse time, (a and c) 70 msec, (b and d) 10 msec; Drop time 0.5 sec.

(6) Width at half height versus log k_a° for differential pulse polarography. Pulse height, (a) 10 mV, (b) 25 mV, (c) 50 mV, (d) 100 mV; Pulse time 10 msec; Drop time 0.5 sec.

(7) Current-voltage curves for differential pulse polarography. Apparent heterogeneous rate constant, (A) 10^{-2} cm/sec, (B) 3×10^{-3} cm/sec, (C) 10^{-3} cm/sec, (D) 10^{-4} cm/sec; Symmetry factor, 0.3.

(8) Log k_a° versus KNO_3 concentration. Determined from normal pulse polarography.

(9) Current-voltage curves of zinc in KNO_3 for differential pulse polarography. Cd 3.37×10^{-5} M, Zn 6.23×10^{-5} M, Drop time 2 sec. Pulse time 16.67 msec, Pulse height 25 mV; (A) 0.1 F KNO_3, reversible electron transfer; (B) 2 F KNO_3, apparent heterogeneous rate constant 2.5×10^{-3} cm/sec, symmetry factor 0.3. (-) simulation (∘) experimental.

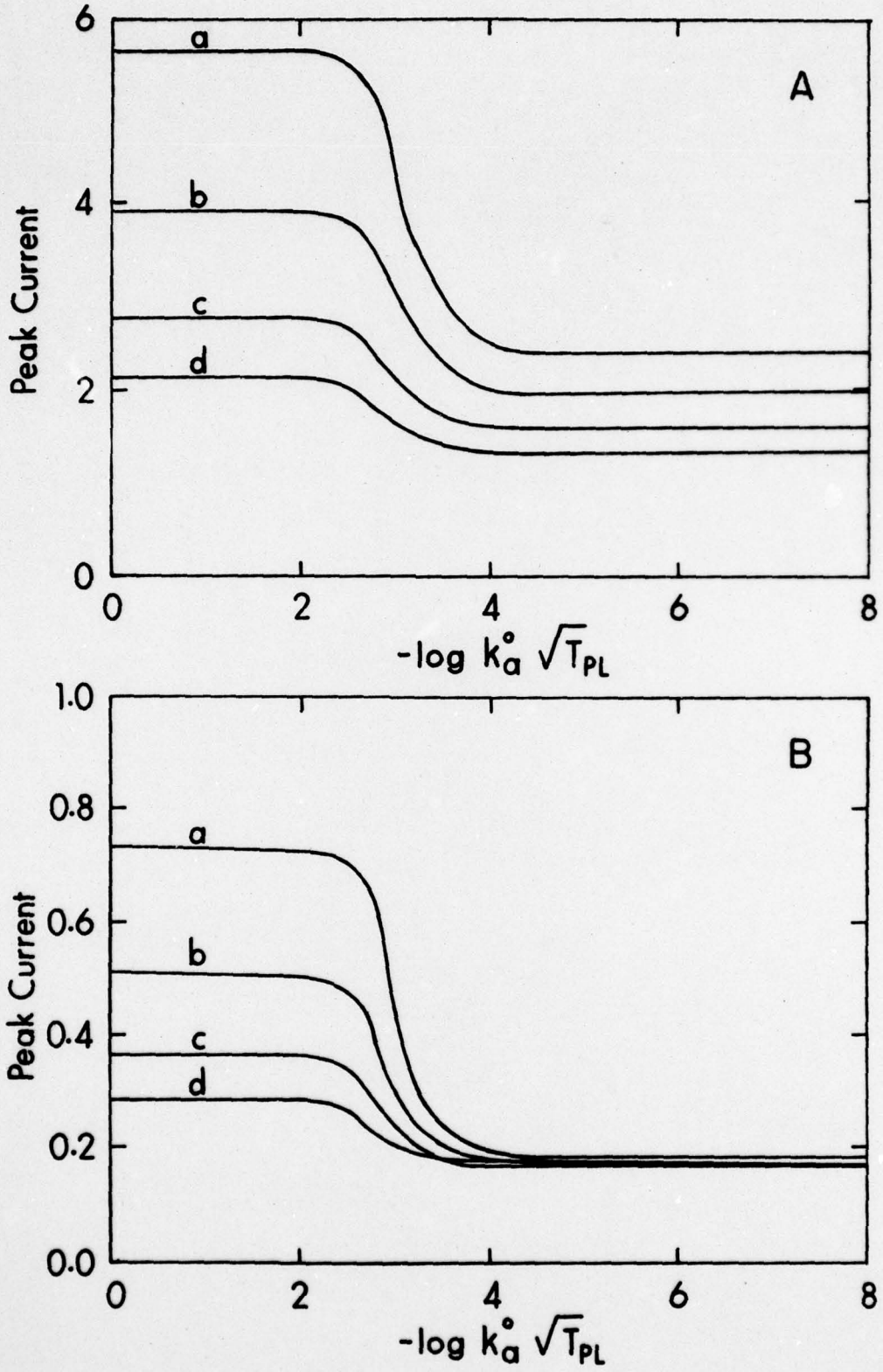
A
B
Peak Current
-log $k_a^\circ \sqrt{T_{PL}}$
a
b
c
d
0
2
4
6
8
0.0
0.2
0.4
0.6
0.8
1.0

FIGURE 1

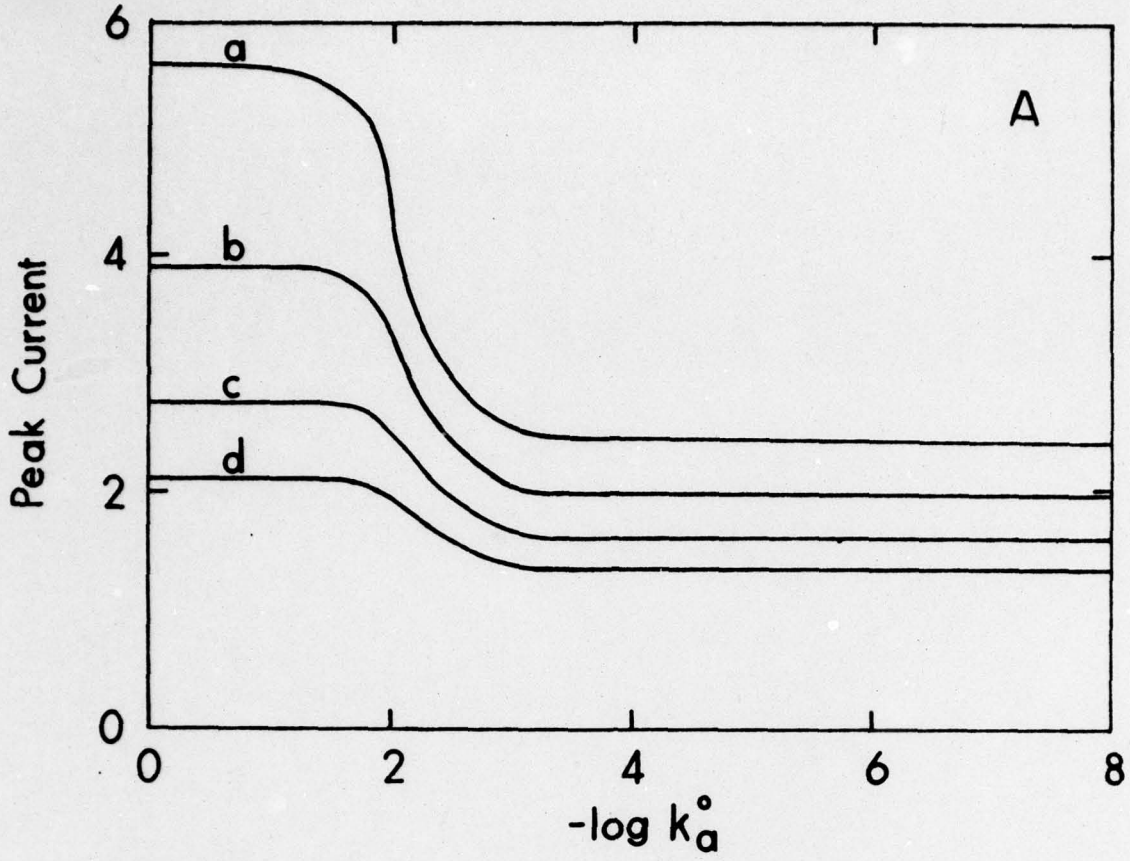
A
Peak Current
6
4
2
0
a
b
c
d
0
2
4
6
8
-log k°a

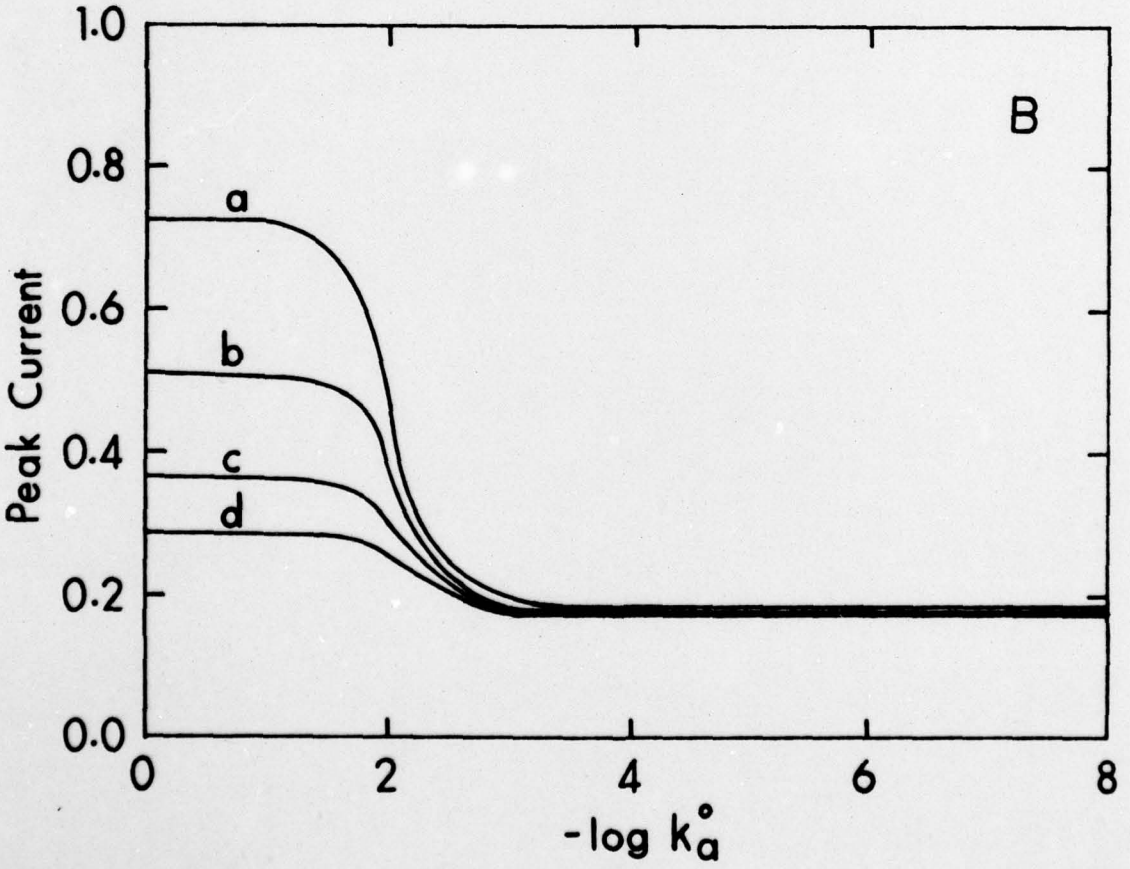
B
Peak Current
1.0
0.8
0.6
0.4
0.2
0.0
a
b
c
d
0
2
4
6
8
-log k°a

FIGURE 2

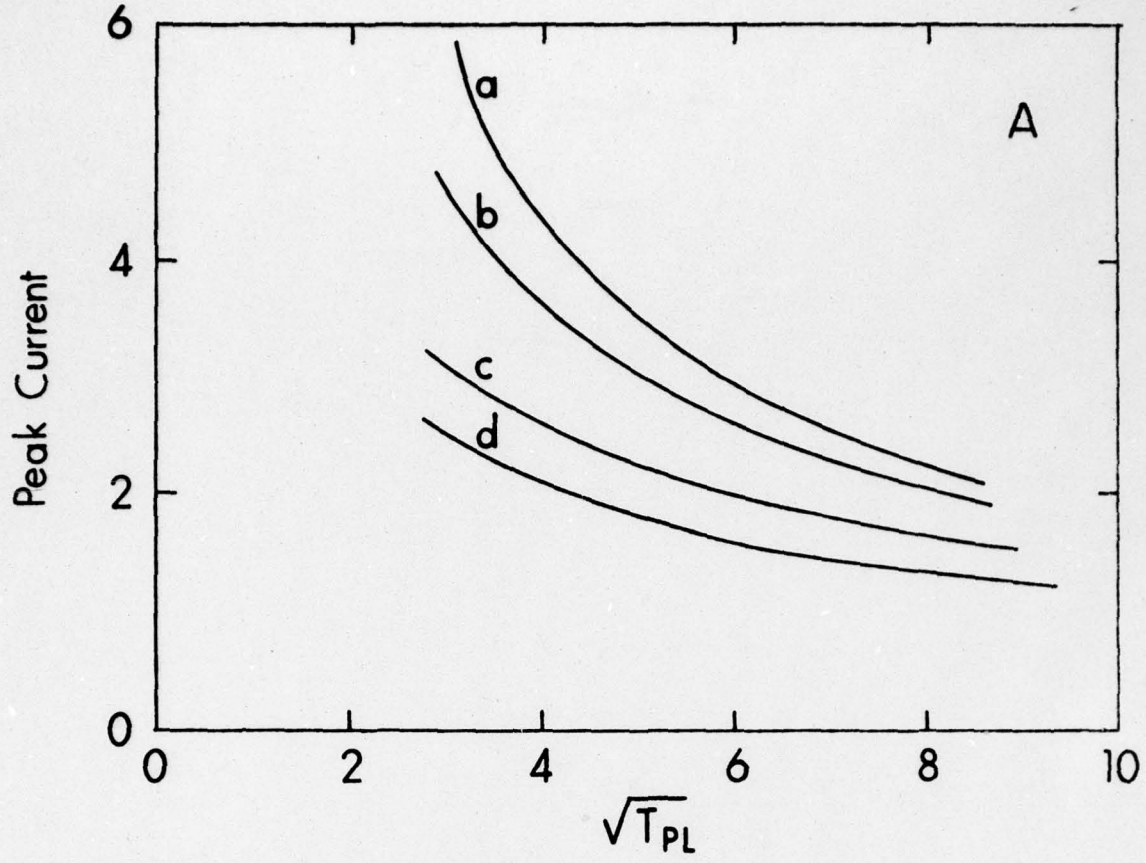
A
Peak Current
6
4
2
0
0
2
4
6
8
10
$\sqrt{T_{PL}}$
a
b
c
d

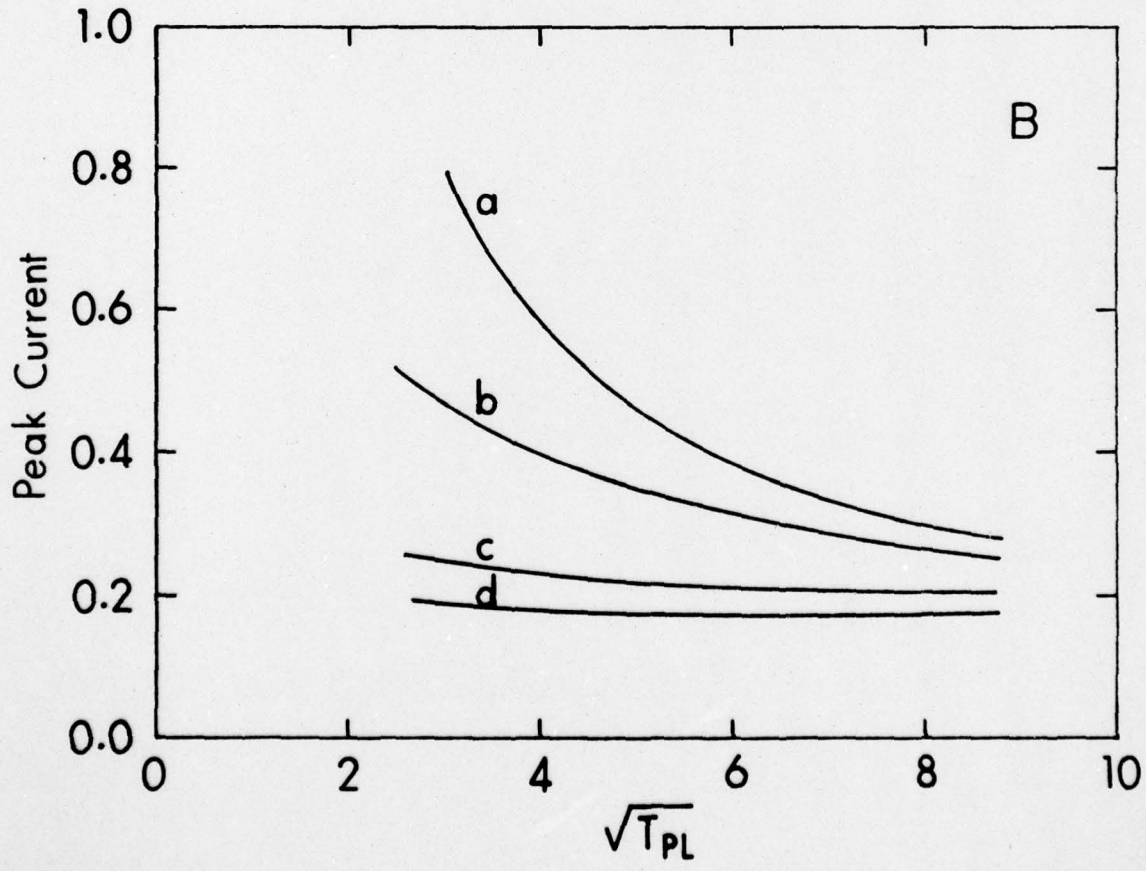
B
Peak Current
1.0
0.8
0.6
0.4
0.2
0.0
0
2
4
6
8
10
$\sqrt{T_{PL}}$
a
b
c
d

FIGURE 3

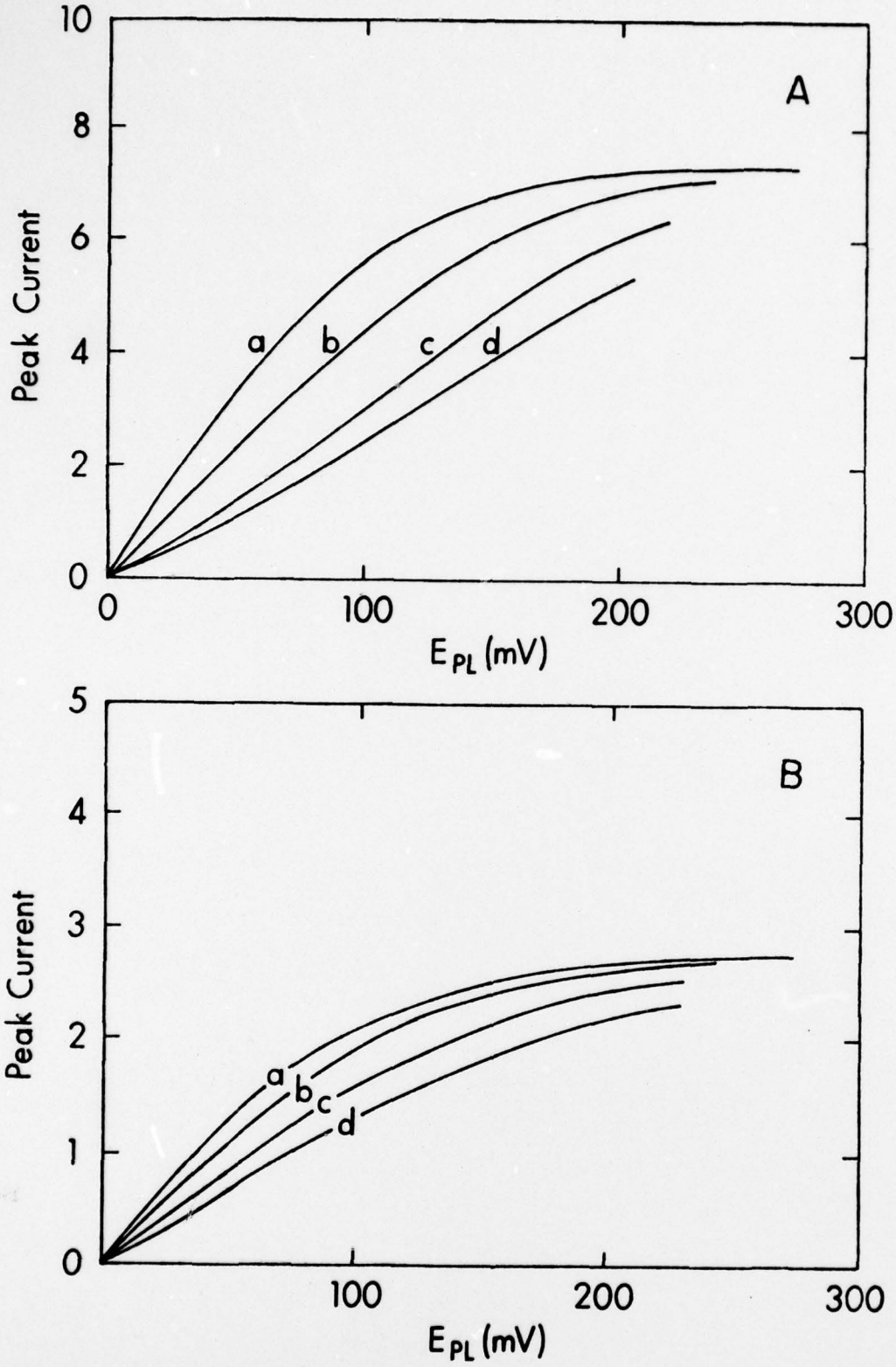
A
Peak Current
10
8
6
4
2
0
a
b
c
d
0
100
200
300
E_{PL} (mV)
B
Peak Current
5
4
3
2
1
0
a
b
c
d
100
200
300
E_{PL} (mV)

FIGURE 4

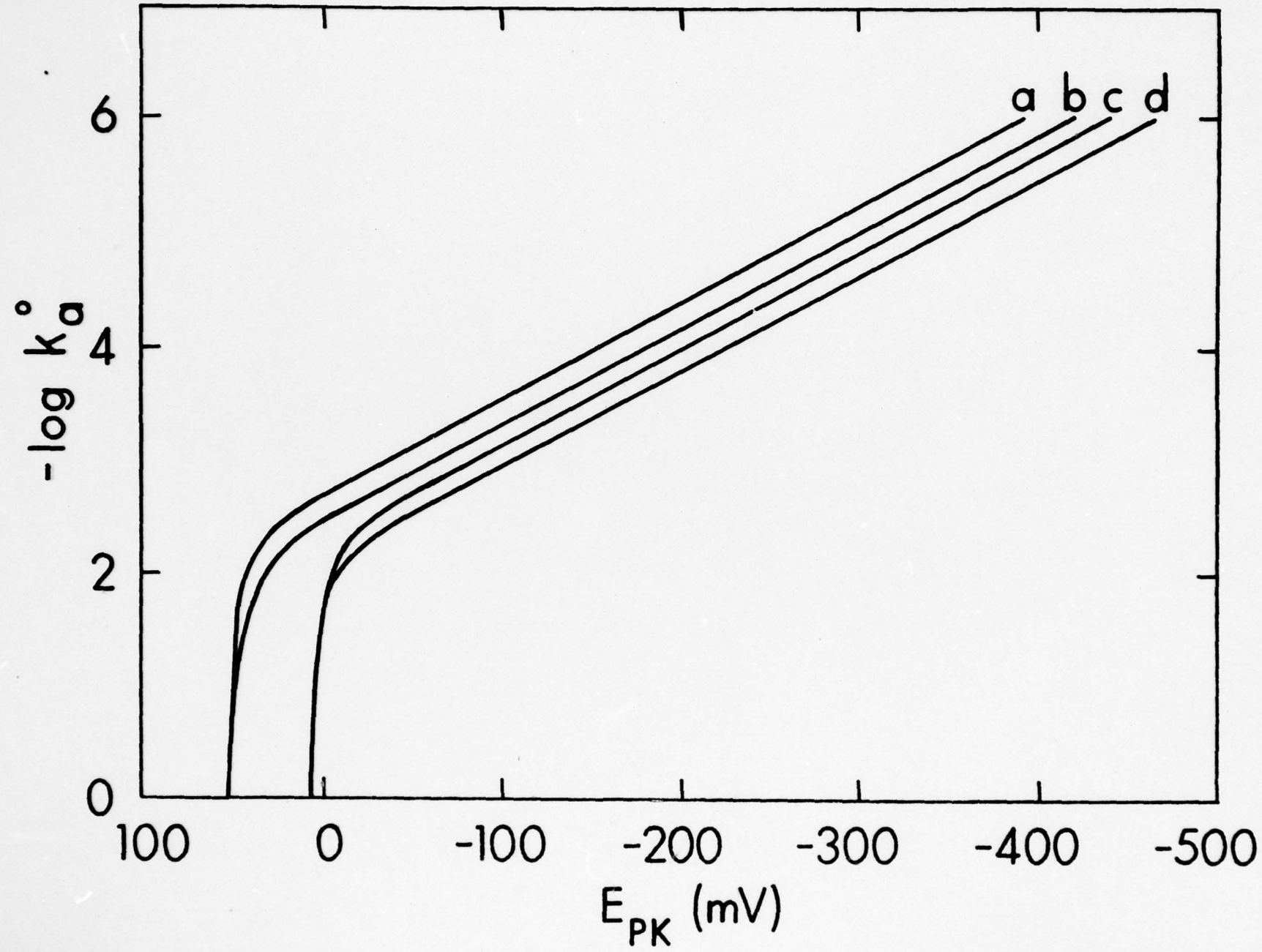

FIGURE 5

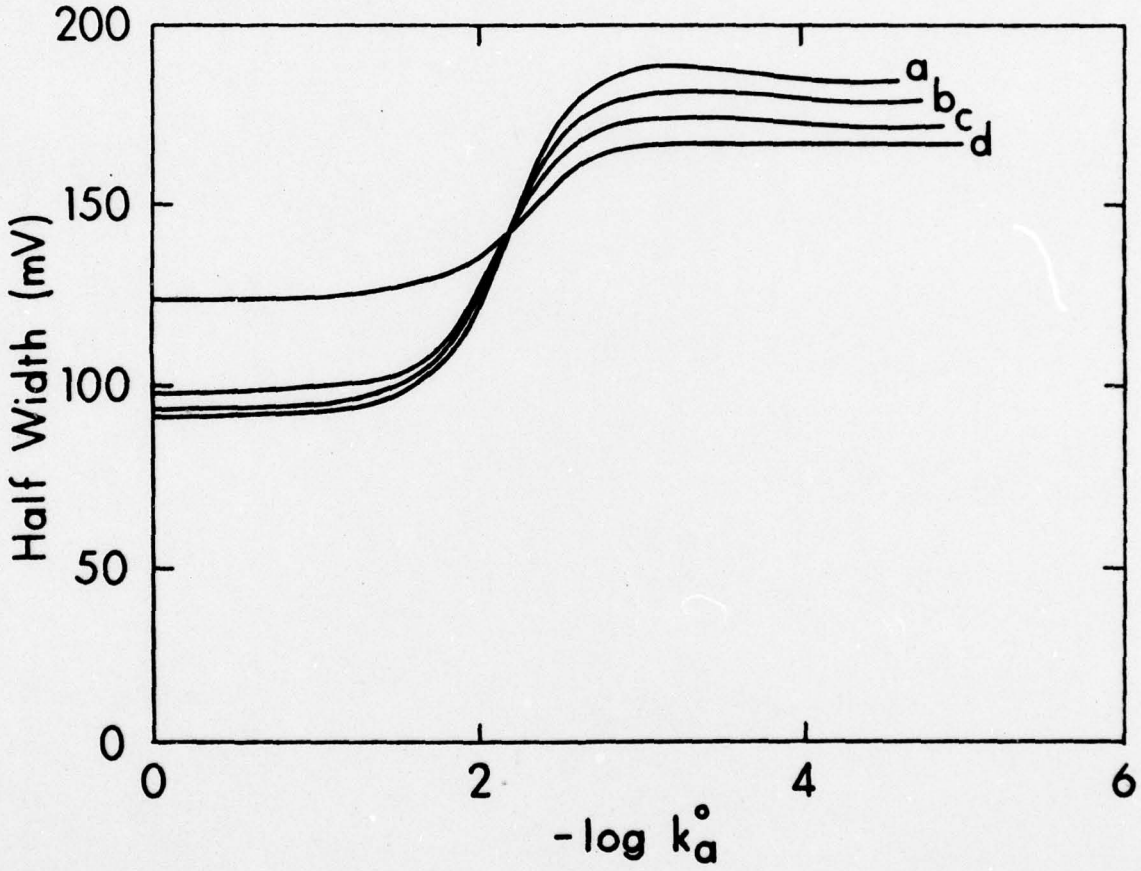

FIGURE 6

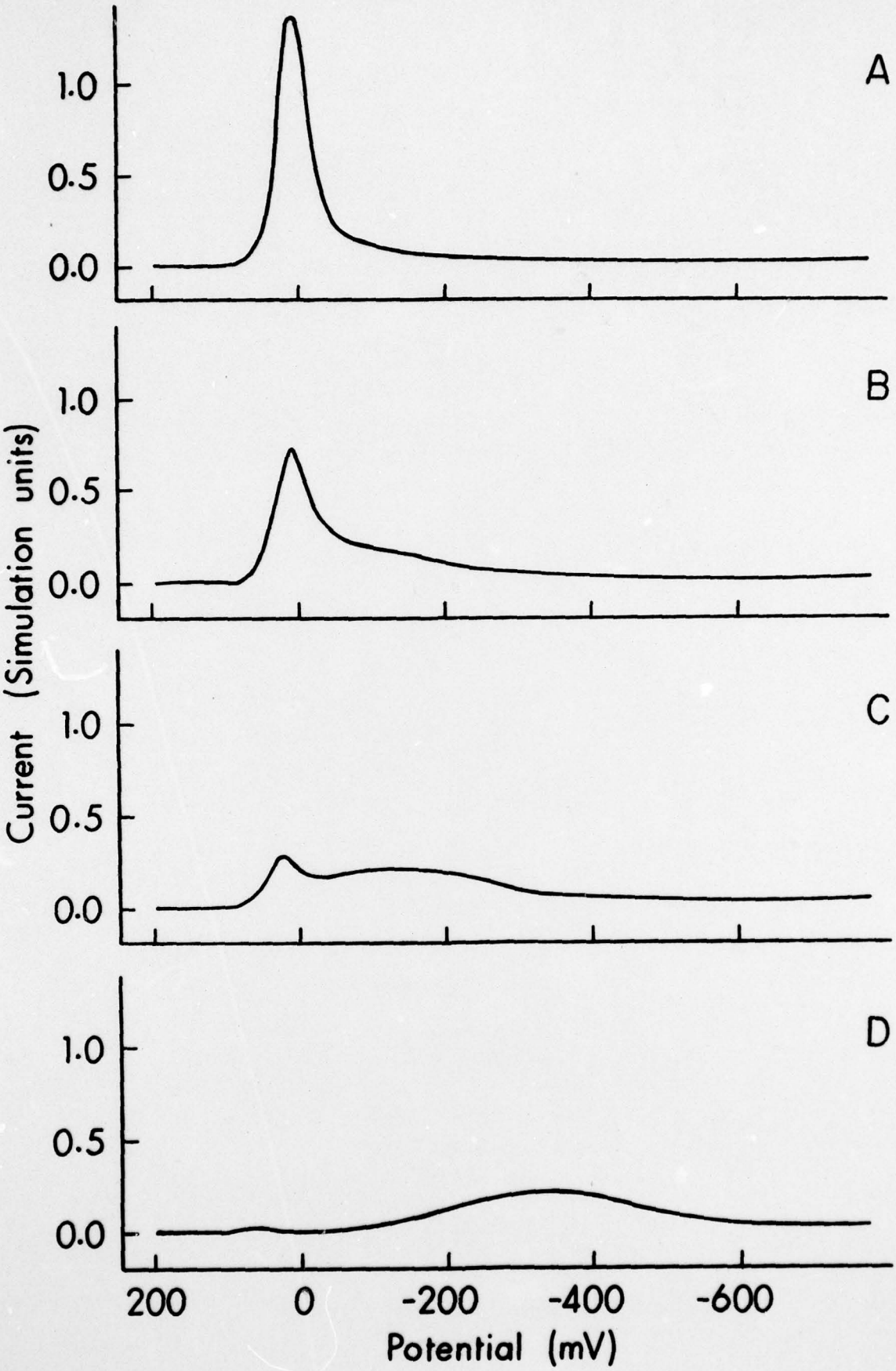
A
B
C
D
1.0
0.5
0.0
Current (Simulation units)
200
0
-200
-400
-600
Potential (mV)

FIGURE 7

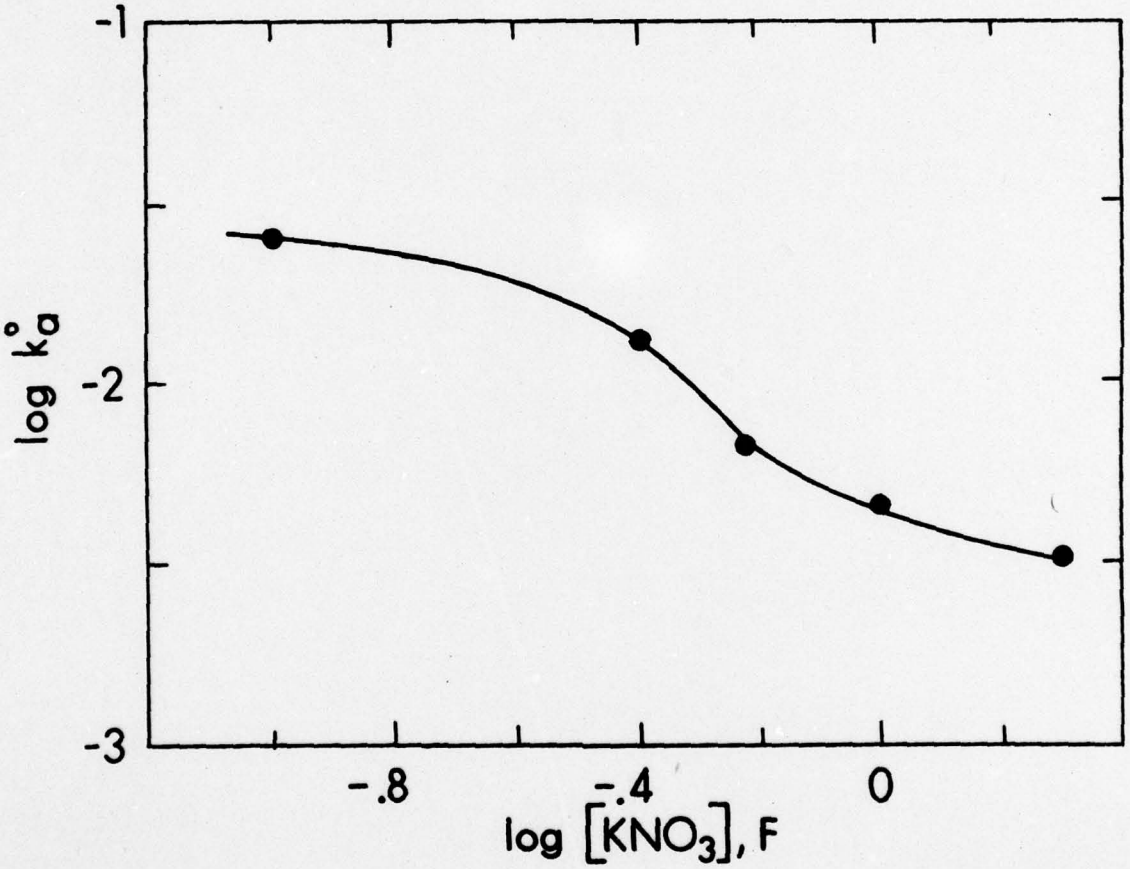

FIGURE 8

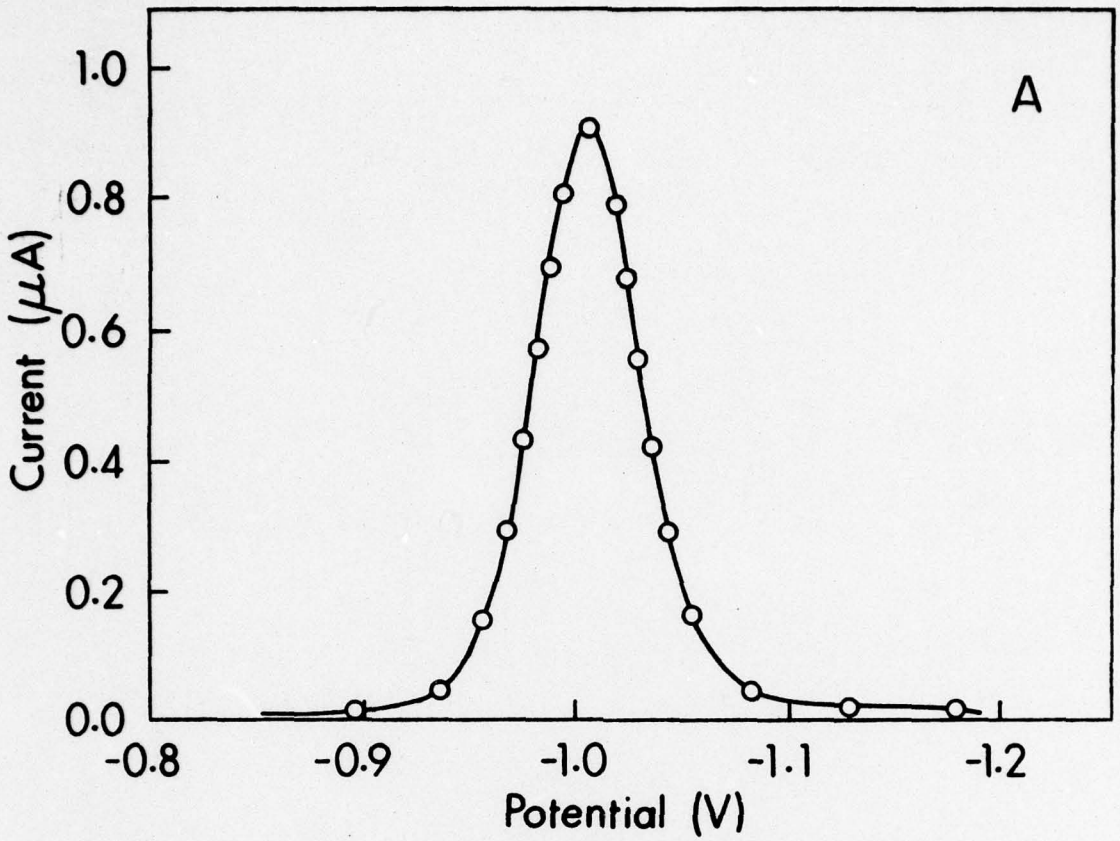
A
1.0
0.8
0.6
0.4
0.2
0.0
Current (μA)
-0.8
-0.9
-1.0
-1.1
-1.2
Potential (V)

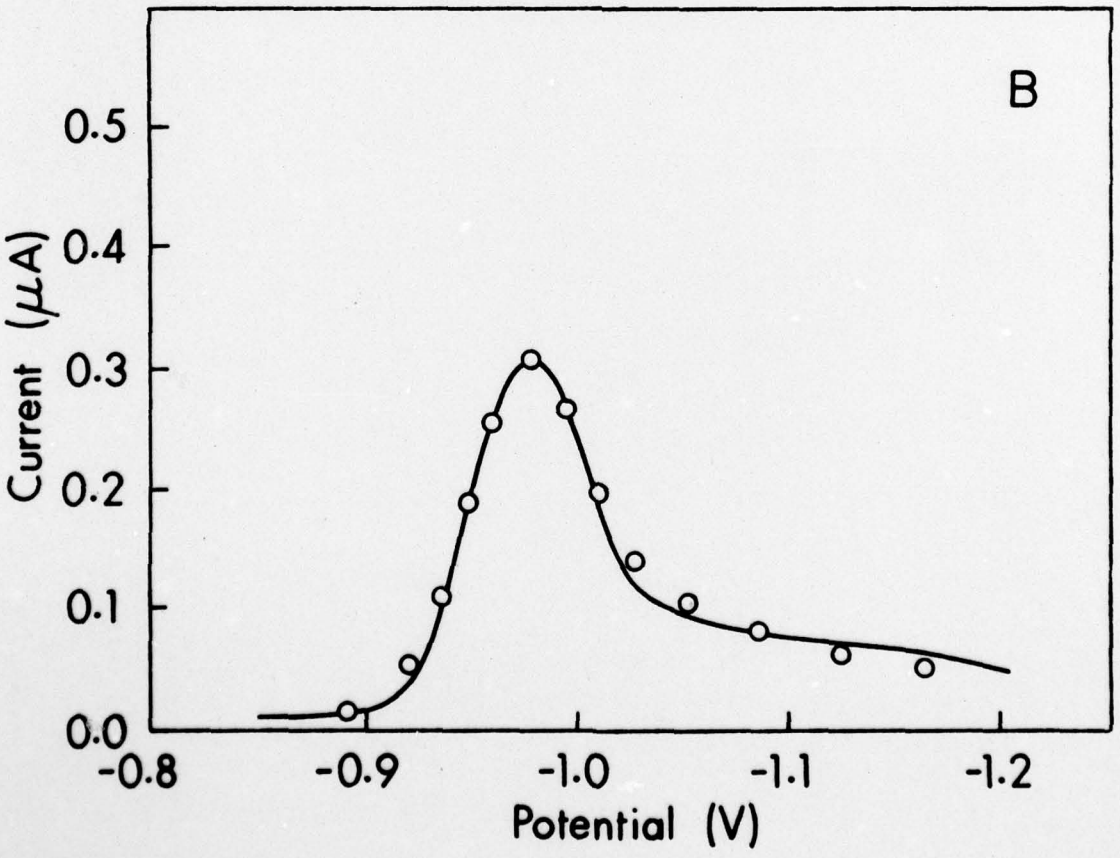
B
0.5
0.4
0.3
0.2
0.1
0.0
Current (μA)
-0.8
-0.9
-1.0
-1.1
-1.2
Potential (V)

FIGURE 9

TECHNICAL REPORT DISTRIBUTION LIST

	No. Copies
Office of Naval Research Arlington, Virginia 22217 Attn: Code 472	2
Office of Naval Research Arlington, Virginia 22217 Attn: Code 102IP 1	6
ONR Branch Office 536 S. Clark Street Chicago, Illinois 60605 Attn: Dr. Jerry Smith	1
ONR Branch Office 715 Broadway New York, New York 10003 Attn: Scientific Dept.	1
ONR Branch Office 1030 East Green Street Pasadena, California 91106 Attn: Dr. R. J. Marcus	1
ONR Branch Office One Hallidie Plaza-Suite 601 San Francisco, California 94102 Attn: Dr. L. H. Peebles	1
Director, Naval Research Laboratory Washington, D. C. 20390 Attn: Code 6100	1
The Asst. Secretary of the Navy (R&D) Department of the Navy Room 4E736, Pentagon Washington, D. C. 20350	1
Commander, Naval Air Systems Command Department of the Navy Washington, D. C. 20360 Attn: Code 310C (H. Rosenwasser)	1
Defense Documentation Center Building 5, Cameron Station Alexandria, Virginia 22314	12
U.S. Army Research Office P.O. Box 12211 Research Triangle Park, N.C. 27709 Attn: CRD-AA-IP	1
Naval Ocean Systems Center San Diego, California 92152 Attn: Mr. Joe McCartney	1
Naval Weapons Center China Lake, California 93555 Attn: Head, Chemistry Division	1
Naval Civil Engineering Laboratory Port Hueneme, California 93041 Attn: Mr. W. S. Haynes	1
Professor O. Heinz Department of Physics & Chemistry Naval Postgraduate School Monterey, California 93940	1
Dr. A. L. Slafkosky Scientific Advisor Commandant of the Marine Corps (Code RD-1) Washington, D. C. 20380	1
Office of Naval Research Arlington, Virginia 22217 Attn: Dr. Richard S. Miller	1

TECHNICAL REPORT DISTRIBUTION LIST

	No. Copies
Dr. M. B. Denton University of Arizona Department of Chemistry Tucson, Arizona 85721	1
Dr. G. S. Wilson University of Arizona Department of Chemistry Tucson, Arizona 85721	1
~~Dr. R. A. Osteryoung~~ ~~Colorado State University~~ ~~Department of Chemistry~~ ~~Fort Collins, Colorado 80521~~	~~1~~
Dr. B. R. Kowalski University of Washington Department of Chemistry Seattle, Washington 98105	1
Dr. I. B. Goldberg North American Rockwell Science Center P.O. Box 1085 1049 Camino Dos Rios Thousand Oaks, California 91360	1
Dr. S. P. Perone Purdue University Department of Chemistry Lafayette, Indiana 47907	1
Dr. E. E. Wells Naval Research Laboratory Code 6160 Washington, D. C. 20375	1
Dr. D. L. Venezky Naval Research Laboratory Code 6130 Washington, D. C. 20375	1
Dr. H. Freiser University of Arizona Department of Chemistry Tucson, Arizona 85721	1

	No. Copies
Dr. Fred Saafeld Naval Research Laboratory Code 6110 Washington, D. C. 20375	1
Dr. H. Chernoff Massachusetts Institute of Technology Department of Mathematics Cambridge, Massachusetts 02139	1
Dr. K. Wilson University of California, San Diego Department of Chemistry La Jolla, California 92037	1
Dr. A. Zirino Naval Undersea Center San Diego, California 92132	1
Dr. John Duffin United States Naval Post-Graduate School Monterey, California 93940	1
Dr. G. M. Hieftje Department of Chemistry Indiana University Bloomington, Indiana 47401	1
Dr. Victor L. Rehn Naval Weapons Center Code 3813 China Lake, California 93555	1
Dr. Christie G. Enke Michigan State University Department of Chemistry East Lansing, Michigan 48824	1
Technical Library P. R. Mallory and Company, Inc. Northwest Industrial Park Burlington, MA 01803	1